



Monte Carlo Simulations of the TelePix 180nm HV-CMOS Pixel Sensor

Sebastian Onder

Vienna University of Technology, Austria

Supervisors: Lennart Huth, Simon Spannagel, Håkan Wennloef

September 7, 2022

Abstract

This study presents a simulations combining three dimensional electrostatic field models simulated in TCAD and Monte Carlo simulations in Allpix² to simulate a 180 nm HV-CMOS pixel sensor. It describes the full Allpix² simulation chain used to carry out the simulations as well as how to incorporate the TCAD models into the Monte Carlo simulations to improve the simulation accuracy.

With the described setup a rotational scan of the pixel detector is simulated to study the behaviour of the sensors performance under rotation. Further, an approach is presented on how to match the simulation results to experimental data that was obtained at the DESY II test beam facility. This approach does not yet yield a simulation fitting the data but provides a basis for further investigations.

Contents

1	Introduction	3
2	The TelePix Pixel Sensor	3
3	Simulation Flow	4
3.1	Geometry	4
3.2	TCAD Import	5
3.3	Charge Carrier Deposition with Geant4	6
3.4	Charge Carrier Propagation	7
3.5	Digitization	8
3.6	Simulation Output and Replay Runs	8
4	Analysis Methods	9
4.1	Observables	9
4.2	Parameter Scans	10
4.3	Comparing Simulations with Experimental Data	11
5	Results	12
5.1	Rotational Scan for 40 μm Thickness	12
5.2	Tuning the Simulations for 100 μm	14
6	Summary and Outlook	15

1 Introduction

The update of the EUDET-type beam telescopes [1] at the DESY II test beam facility [2] has led to the development of novel pixel sensors purposed to provide improved beam reconstruction in the reference telescope based on the MIMOSA26 sensors [3, 4]. One such pixel sensor currently under study is the TelePix, which is supposed to provide additional timing information on particle tracks created by electrons from the DESY II accelerator. With a time resolution of < 5 ns the TelePix is supposed to supply the telescope with track time stamping as well as a configurable region-of-interest trigger. While there are existing laboratory characterizations for the TelePix, simulations are of significant importance as well, since they allow to make predictions about the performance of the sensor with less extensive data analysis and resources. For this purpose the simulation framework Allpix² [5] offers a toolbox for the virtual characterization of silicon detectors. Further Allpix² detector simulations produce similar performance and analysis observables as the monitoring and analysis software at the DESY II test beam facility. This makes a comparison of experimental data acquired through measurements of the TelePix at the test beam and simulated data very convenient.

The Allpix² framework offers simulation tools reaching from particle energy deposition via Geant4 [6–8], Monte-Carlo simulation of the charge carrier propagation through the detector material as well as the capability to import electric fields and doping profiles simulated via TCAD. This gives the possibility to develop simulations that imitate the physical processes in silicon detectors as well as real life measurements. The effectiveness of Allpix² can be seen in [9], which presents an approach combining TCAD simulations of a sensors electrostatic fields with Allpix² Monte Carlo simulation of charge carrier deposition, transport, collection and signal digitization to match experimental data with great precision. This study adopts an adapted but similar simulation flow, while focussing on the simulations in Allpix².

This report is structured as follows. Section 2 will explain the TelePix sensor in more detail, while Section 3 describes the simulations in Allpix². Section 4 looks at the methods used to analyse the simulated detectors performance as well as methods to tune simulation and test beam data. 5 shows the simulation results and 6 contains a summary, conclusions and closing remarks.

2 The TelePix Pixel Sensor

The TelePix sensor is a monolithic active pixels sensor (MAPS) proposed as a part of the EUDET beam telescope updates at the DESY II test beam facility. With a time resolution of < 5 ns the TelePix provides track timestamping and a region of interest trigger to prevent ambiguities in the readout of the MIMOSA26 reference telescope sensors at high particle rates.

The basic active sensor layout is comprised of a 29×124 pixel array with a pitch of $165 \times 25 \mu\text{m}^2$ and thickness of $100 \mu\text{m}$ for each pixel. As a MAPS the readout electronics of the TelePix is integrated on the same silicon wafer as the active pixel layout. This sig-

nificantly reduces the overall material budget when compared to the widely used hybrid architectures, where the readout electronics sit on a separate chip and attached to the active sensor wafer via bump bonding. By further using an 180 nm HV-CMOS process the individual pixel size can be reduced to as well while keeping a thick active depletion layer at bias voltages up to 100 V and a bigger collection electrode with respect to the pixel pitch to accelerate charge collection.

3 Simulation Flow

This section provides a look on the Allpix² simulation chain and parameters used to simulate the TelePix sensor. Allpix² simulations are built from a set of modules that each simulate specific physical processes or assist the operator by e.g. reading/writing data from/to memory or recording the simulation results in plots and histograms. These modules require parameter specifications written in configuration files, which are provided to the framework at the start of a simulation run. The run then consists of several events, where in each event the whole simulation chain is processed. This study uses for every run 250000 events.

While custom modules can be designed and integrated into the Allpix² framework, this study only uses the modules provided in the default installation of version 2.3.1 [10].

In the course of this section the used modules as well as their relevant parameters are described step by step.

3.1 Geometry

Since a single TelePix pixel is heavily asymmetric in its dimensions ($165 \times 25 \times 100 \mu\text{m}$) it is necessary to define the assumed orientation of the detector in an arbitrary coordinate system (simulation or laboratory). Fig. 3.1 shows a TCAD simulation of the electric field magnitude of the top $40 \mu\text{m}$ of a single TelePix pixel in three dimensions as well as the orientation in the coordinate system. So for the remainder of this paper it is assumed that the full thickness of $100 \mu\text{m}$ of the pixel is oriented along the z -axis, the longer side of $165 \mu\text{m}$ lies in the x -direction and the shorter side of $25 \mu\text{m}$ in the y -direction.

For the simulations in Allpix² the `GeometryBuilderGeant4` module provides an interface to Geant4 and handles constructing the basic detector geometry, volumes and materials in the internal coordinate system of the simulation. The aforementioned pitch and number of pixels is provided by a model configuration file, which can be seen in Listing ?.

The whole sensor is centered in the origin of the Allpix² coordinate system and is comprised of an 29×124 matrix of directly adjacent pixel cells. Each pixel cell is equipped with an collection electrode implant centered on the surface of every pixel. The implant volume is defined as $150 \times 15 \times 7.5 \mu\text{m}$ in x -, y - and z -direction respectively.

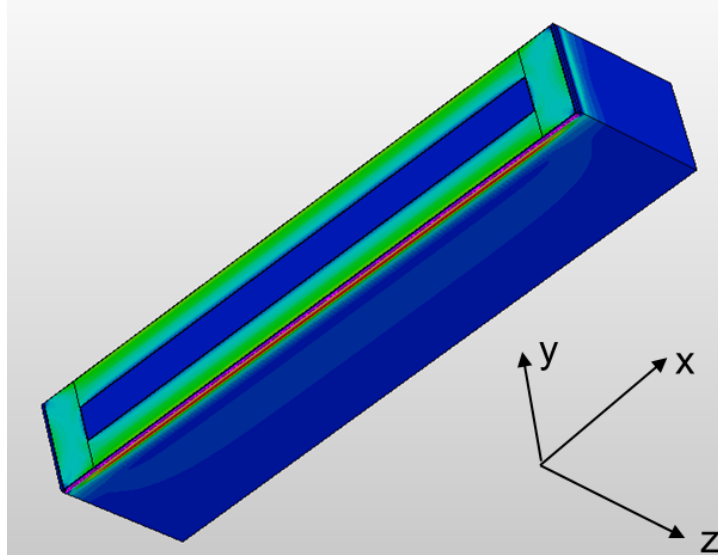


Figure 1: asf

3.2 TCAD Import

TCAD is a widely used software tool to model and simulate manufacturing processes as well as electric properties of semiconductor devices, such as silicon detectors. Allpix² on the other hand provides the possibility to import electrostatic field and doping profiles simulated in TCAD. Thus the simulation of charge carrier drift and diffusion as well as recombination in Allpix² can be imitated more accurately and true to the real world physical processes. The import is handled respectively by the `ElectricFieldReader` module for the electric field and the `DopingProfileReader` module for the doping profile. The three dimensional TCAD profiles such as the one shown in Fig. 3.1 have periodic boundaries at the edges. Thus every individual pixel can be filled with the field profile across the whole pixel matrix without a break in continuity at pixel edges. The low field region in blue on the surface of the cell is the top of the collection electrode. A high field around the top edges is created by a p-stop ring.

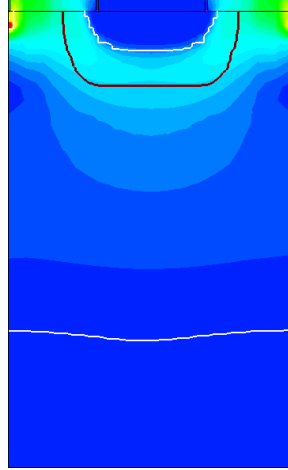
Fig. ? shows the electric field obtained in TCAD of the top 40 μm of a TelePix pixel as cross-sections in the x - z -plane and y - z -plane respectively.

The white lines indicate the depleted volume in the pixel near the pn-junctions at the electrode and the p-stops in the corners. The brown lines indicate the collection electrode volume. Here the high electric field induces a drift of the electrons along the field lines towards the collection electrode. The high electric field regions at the electrode and p-stops rapidly decreases along the z -axis at the edges of the depleted region and towards the backside of the pixel. Here the charge propagation is mostly impacted by diffusion. But also recombination gets a relevant factor as the doping concentration is higher in the non-depleted region.

Since TCAD simulations use irregularly spaced meshing of points in the material, the



(a) caption



(b) caption

Figure 2: asf

`Mesh Converter` tool provided by Allpix² has to be used to convert the TCAD profiles into regular spaced meshes before the import into Allpix² simulations. The chosen granularity of the converted mesh is $0.1\ \mu\text{m}$.

3.3 Charge Carrier Deposition with Geant4

Via the `DepositionGeant4` module the energy deposition of incoming particles can be simulated through an interface to Geant4. To simulate the TelePix under the same conditions as for the test beam measurements a $5\ \text{GeV}$ electron beam source is used. One simulation event simulates one single electron hitting the detector.

Fig. 3.3 shows a visualization of the sensor geometry with an electron track (one event) propagating through the sensor as well as the orientation in the coordinate system. The beam is centered around the z -axis and has a sharp Gaussian profile with a small width of $150\ \mu\text{m}$ to prevent events from missing the detector as well as different charge sharing behaviour around the sensor edges. As radiation damage is not simulated, every pixel is essentially identical over all events. The beam width will therefore have no impact on the detector performance as long as no particles miss the detector. The simulation also considers a model for Photo-Absorption Ionization (PAI) for more accurate modelling of the energy deposition in thin sensors as the most part of the signal stems from charge

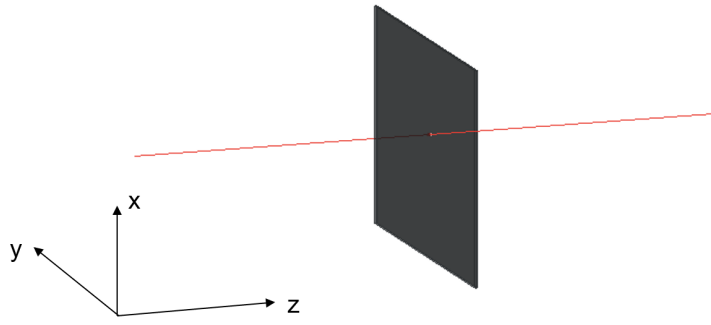


Figure 3: asf

carriers created in the depleted volume, which is significantly thinner than the actual sensor thickness.

3.4 Charge Carrier Propagation

Charge carrier propagation is handled by the `GenericPropagation` module. Fig. 3.4 shows a visualization of the charge carrier propagation in Allpix² in a so called linegraph. Each line represents the propagation path of a group of electrons until the end of the simulation. The cloud in the lower portion corresponds to random diffusion movement in the undepleted volume of the sensor. The more or less straight tracks pointing towards the cloud on the surface, where the collection electrode is located, are charge carriers drifting along the electric field lines.

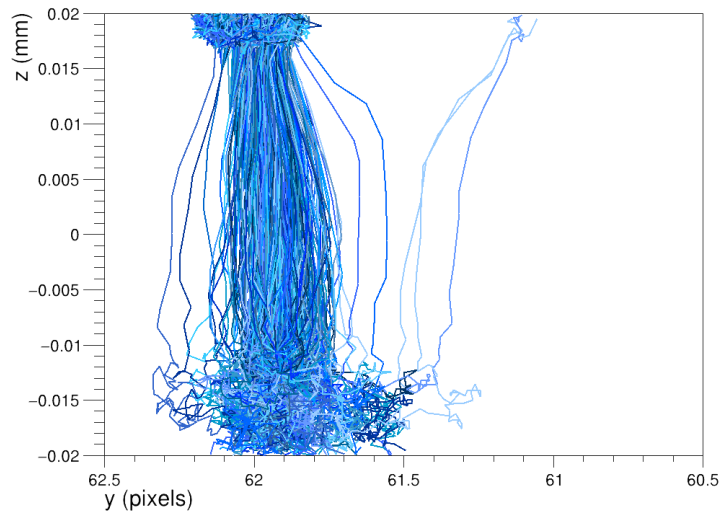


Figure 4: asf

The simulation process of the propagation is divided into several time steps. At every

step Allpix² considers a combination of a physical mobility model and the electric field to determine the charges' movement via random diffusion and drift along electric field lines. Here the Masetti-Canali mobility model (see [10]) is employed to simulate the transport.

As charge carriers can also recombine with atoms in the substrate, a recombination model is employed as well to emulate this process. The used model is the SRH-Auger recombination model (see [10]).

The range of time step lengths is set to $0.5 \text{ ps} \leq \Delta t \leq 50 \text{ ps}$. Every step propagates a group of 5 charge carriers at once to speed up the simulations. After an integration time of 25 ns (default value) the propagation simulation is halted.

Since single pixels are positioned in a matrix adjacent to other pixels, charge carriers deposited in one pixel can propagate to the electrode of a neighbouring pixel. This can also be seen in Fig. 3.4, where the majority of the charge carriers is collected on an electrode to the right while a few single charge carriers are collected in an electrode to the left. This further enables charge sharing. Charges that end up in the collection electrode volume of a pixel are then attributed to the signal of the corresponding pixel.

3.5 Digitization

After charge collection at the collection electrodes the `DefaultDigitizer` module simulates digitization of the signal in readout electronics. The module first adds random electronics noise to the collected charge at every pixel, which stems from a Gaussian distribution with a mean of 0 e and a width that can be specified via the `electronics_noise` parameter in units of electrons. Also a multiplication factor simulating an amplifier specified in the `gain` parameter is applied to the signal charge afterwards. The resulting signal charge is then compared to a threshold per pixel, which is specified through the `threshold` parameter in units of electrons as well.

If the collected signal charge is higher than a pixels threshold, the pixels readout is triggered and a pixel hit is detected. For every pixel hit a threshold uncertainty is applied as well, which also comes from a random Gauss distribution with a mean of 0 e and width of 5 e specified in the `threshold_smearing` parameter..

3.6 Simulation Output and Replay Runs

Allpix² uses the `ROOTObjectWriter` module to write the simulation output to ROOT [11] files and trees. The output entails on the one hand the simulation results produced by all the modules recorded in several histograms, which can be used for physics and performance analysis. On the other hand also the Monte Carlo truth information of all the simulation processes can be recorded and written to a file.

The latter can be used to significantly speed up the simulations by dividing the simulations into two steps. First a base simulation run with a fixed random seed is carried out. Afterwards the Monte Carlo truth output can again be imported via the `ROOTObjectReader` to essentially repeat the simulation events from the base run in a

so called replay run. Since the already simulated events from the base run do not have to be calculated again, a replay run where e.g. only one parameter in the configuration is changed — such as the digitizer threshold — can be performed significantly faster (speed up of threshold scans, see section 4.2).

4 Analysis Methods

The following section describes the methodology to test the behaviour and performance of the simulated detector setup discussed above as well as the observables which are analyzed in order to accomplish that. Further methods to tune the simulation to match real life data measured at the DESY II test beam facility are discussed.

4.1 Observables

Through the recorded Monte Carlo truth information for a simulation run, Allpix² is able to provide a reference to the track reconstruction of incoming particles produced by the simulated detector. The `DetectorHistogrammer` module compares the Monte Carlo truth and reconstructed information in order to produce measures and observables, which describe the simulated detector’s performance and records them in histograms. This study focuses on three performance observables in particular: efficiency, spacial resolution and mean cluster size.

First off, the efficiency is a percentage measuring the capability of a detector to detect an event, i.e. an incoming particle hitting the detector. It is calculated by dividing the number of events detected by the investigated detector over the total number of simulated events (or events detected by a reference beam telescope).

The spacial resolution with the dimension of length, is the systematic uncertainty attributed to a reconstructed particle hit position on the sensor. It is obtained by statistical analysis of so called track residuals. Residuals are the difference of the reconstructed hit position of an incoming particle in the horizontal plane (x - y -plane) and the true hit position. Filling a histogram with the residuals for every event (residuals on the horizontal axis) yields a residual distribution. It is important to note that residuals are calculated in x - and y -direction respectively. By further looking at the standard deviation of the resulting residual distribution the spacial resolution in x - and y -direction are obtained. The third important observable is the cluster size or more specifically the mean of the cluster sizes obtained over all events. A pixel cluster consists of one or several adjacent pixels, which respectively collect charge higher than the specified threshold in the course of an event triggering their readout (pixel hit). The cluster size then specifies the number of triggered pixels in the cluster. It has to be noted that there can be several clusters per event.

Through clustering the pixel detector is able to more accurately reconstruct an incoming particle’s hit position on the detector by determining the clusters center of gravity. Through weighting the pixel’s influence on the center-of-gravity position by the individual collected charge that has been shared between the pixels in a cluster (charge

weighting), an even more accurate position reconstruction and lower resolution can be acquired.

Due to charge sharing and weighting it can be predicted that the optimal position reconstruction and resolution can be obtained for a cluster size of 2. This follows from the idea that for a cluster size equal to one there cannot be said exactly where the incoming particle hit the single pixel and for cluster sizes higher than 2 the area of possible hit positions gets bigger, while the area of possible hit positions is closely confined to the edges between two pixels for a cluster size of 2. Reaching a mean cluster size of 2 over all events at a high efficiency is therefore desirable to optimize the performance of a detector in simulations as well as experimental studies.

4.2 Parameter Scans

In order to find the optimal detector performance one has to study the behaviour of the aforementioned observables under the change of parameters in the simulated setup. Parameter scans are a series of simulation or measurement runs where specific settings in the setup are changed in each run. In the case of this study the changing parameters are the digitizer threshold as well as the incidence angle of the incoming particles on the detector as they significantly affect the detection performance.

Higher thresholds may help in filtering uninteresting events with low electron yield and low cluster size, therefore bettering the overall resolution. Too high thresholds although result in a decline of efficiency since the number of detected events decreases.

Changing the incidence angle of particles with respect to perpendicular incidence on the other hand has effect on the particle's track length through the detector. Higher angles result in longer tracks, which will lead to a higher amount of charge carriers in the material, increasing the detection probability and as a result also the efficiency. Further the mean cluster size can be controlled directly since the particle can traverse through several pixels. So it can be expected that at a specific angle and operated with a specific threshold the detector yields a mean cluster size of 2 and therefore an optimal resolution.

To find these optimal parameters, a rotational scan around the x -axis is performed i.e. separately measuring the detectors performance at different discrete angles with respect to perpendicular particle incidence. For every single angle also a threshold scan is run i.e. the performance is measured for different discrete threshold values before the angle is changed. The threshold scan simulations take advantage of simulation replays as discussed in section 3.6, while for each new angle there has to be run a new base simulation.

The simulated angles for the initial rotational scan reach from 0° to 60° with a step size of 5° . At every angle simulation replays with thresholds from 400 e to 3000 e with a step size of 200 e. For that a TCAD field with a resistivity of $200 \Omega \text{ cm}$ at a bias voltage of -80 V and only simulating the top $40 \mu\text{m}$ of the full thickness of a pixel is used. The assumption is that the majority of the signal is created in the depleted volume, thus simulating only the top of the pixel is sufficient. Even if the results do not match

the reality, the scan helps in understanding the general behaviour of the sensor under rotation and in seeing if said behaviour matches expectations. The results can be seen in section 5.1.

4.3 Comparing Simulations with Experimental Data

Comparing data from experimental measurements and simulations allows to analyze the simulations ability to imitate the actual hardware, which was tested experimentally and update the simulation accordingly if the match is not sufficient. In the case of this study the efficiency and the cluster size are the key observables used to compare the performance.

The data that was obtained for the comparison stems from measurements at the DESY II test beam facility. For that the EUDAT-type beam telescopes based on the already mentioned MIMOSA26 sensors are used. The sample TelePix sensor was placed on a rotatable pedestal to perform a rotational scan around the x -axis. Although only cluster size and efficiency data for a threshold scan at an angle of 25° have been analyzed sufficiently to make a comparison. Fig. 4.3 shows the cluster size histogram of the measurement at 25° . At this angle the data shows a desirable mean cluster size of 1.998.

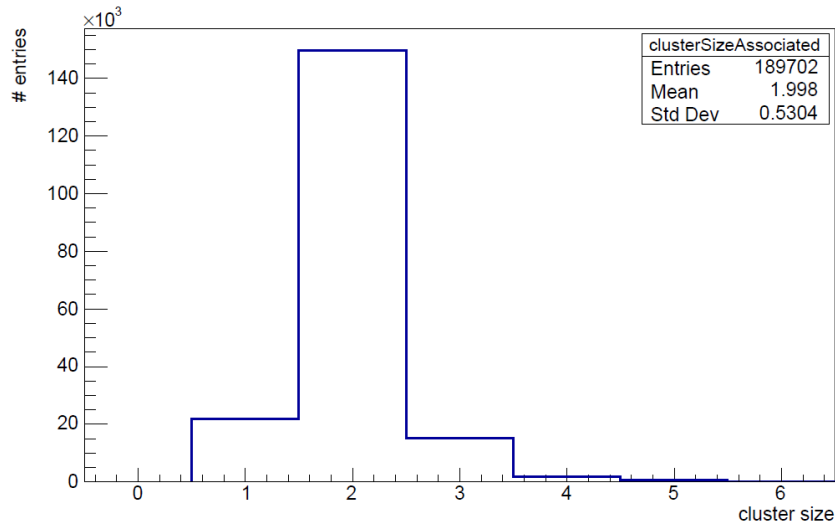


Figure 5: asf

As a first approach to match the simulations to the data threshold scan simulations with two different TCAD input profiles at 25° were performed. Both fields fill pixel cells with the full pixel thickness of $100\ \mu\text{m}$, but differ in their doping profile with a resistivity of $200\ \Omega\ \text{cm}$ and $400\ \Omega\ \text{cm}$ respectively. A comparison of the cluster size with the data yields which resistivity is to prefer.

The preferred field then is more closely analyzed via fine tuning the digitizer setup in the configuration. The parameters used to tune the curves are the electronics noise and

the gain, which are described in section 3.5.
 The results can be seen in section 5.2.

5 Results

This section presents the results from the rotational scan described in section 4.2 and the results from comparing the simulations to the data 4.3.

5.1 Rotational Scan for 40 μm Thickness

Fig. 5.1 shows the efficiency versus the threshold at different beam incidence angles. Only every tenth angle is shown for the sake of visibility.

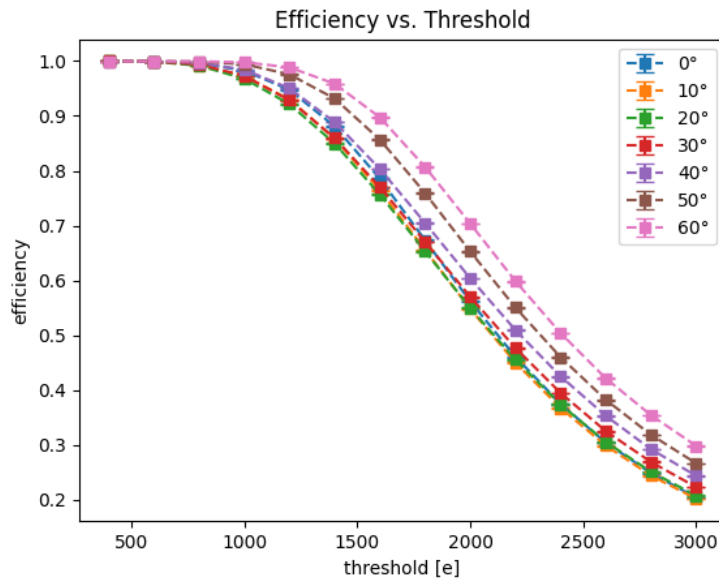


Figure 6: asf

The efficiency curves show the expected “s”-shape i.e. a small drop in efficiency for lower thresholds changing into an almost linear dependence with growing threshold and going towards zero afterwards. It can also be seen that the curves seem to spread with growing angles, meaning a higher angle results in a shift to the right and overall higher efficiency for every threshold. This also matches expectations since at higher angles more charge carriers are produced increasing the detection probability. Although it has to be noted that at lower angles and thresholds the shift is not really noticeable since the overall efficiency at 0° seems to be a bit higher than the one for e.g. 30°. This could be due to statistical fluctuations in the Monte Carlo processes, as well as the fact that the mean cluster size has not yet changed a lot for these simulations.

Fig. 5.1 shows the resolution along the y -axis versus the beam incidence angle for two different thresholds, namely 400 e and 2200 e.

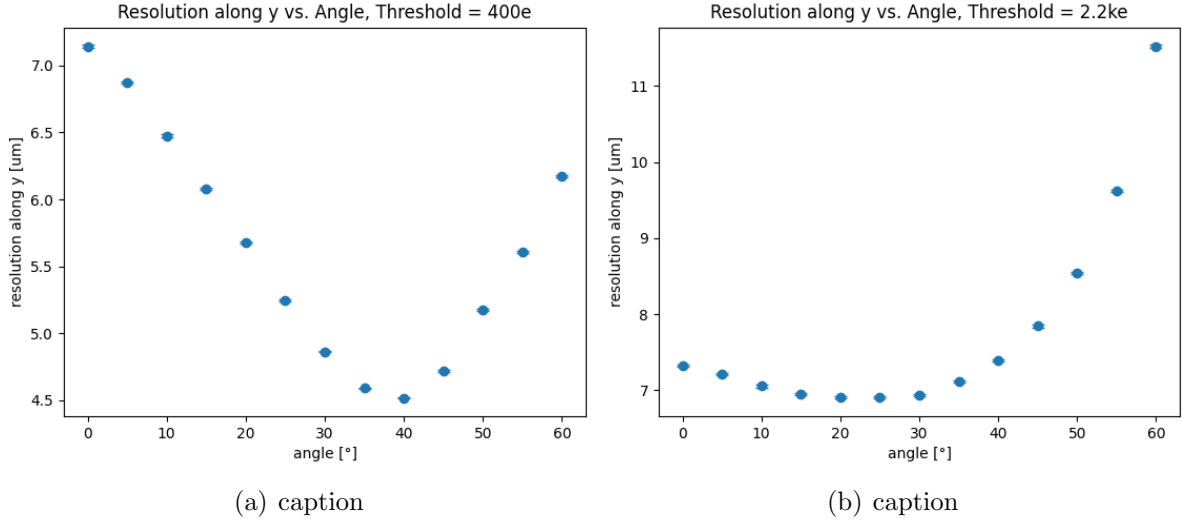


Figure 7: asf

Both plots show a minimum at a specific angle: 40 $^\circ$ for a threshold of 400 e and 25 $^\circ$ for a threshold of 2200 e. At these thresholds these would be the optimal angles, where the best spatial resolution in y -direction can be found. Though Fig. 5.1b strongly suggests that there might be a better angle between 20 $^\circ$ and 25 $^\circ$.

The shown behaviour of the resolution matches expectations as well, as the with growing angle the mean cluster size approaches a value of two, which results in the decrease of resolution. As soon as the cluster sizes gets higher than 2 the resolution increases again. The mean cluster size found at the minimum resolution for a threshold of 400 e is at 1.754, indicating that there is an angle with even lower resolution between 35 $^\circ$ and 45 $^\circ$. For a threshold of 2200 e the mean cluster size at the minimum resolution is 1.03. This shows that at very high thresholds it might not be possible to reach a mean cluster size of 2 as the shared charge at single pixels is too low compared to the threshold. This is also backed by the fact that the efficiency at a threshold of 2200 $^\circ$ has gone down to around 0.5 to 0.6 for all simulated angles as indicated by Fig. 5.1.

Overall the observed behaviour of the results from the rotational scan match expectations. Although they do not match reality as the test beam results shown in Fig. 4.3 suggest that an optimal angle of 25 $^\circ$ can actually be found with a significantly lower threshold already, namely 1099 e. As a comparison the simulation for a threshold of 1000 e yields a optimal angle of 45 $^\circ$ with a mean cluster size of 1.399. How to improve the match to the test beam data is described in the following section.

5.2 Tuning the Simulations for $100\ \mu\text{m}$

Fig. 5.2 shows the simulated cluster size histograms for 4 simulation setups all using the full $100\ \mu\text{m}$ pixel thickness. The top row shows simulations for a threshold of $400\ \text{e}$, while the bottom row was simulated with a threshold of $1100\ \text{e}$. The simulations in Fig. 5.2a and Fig. 5.2c however use TCAD profiles simulating a resistivity of $200\ \Omega\ \text{cm}$, while the ones for Fig. 5.2b and Fig. 5.2d have a resistivity of $400\ \Omega\ \text{cm}$.

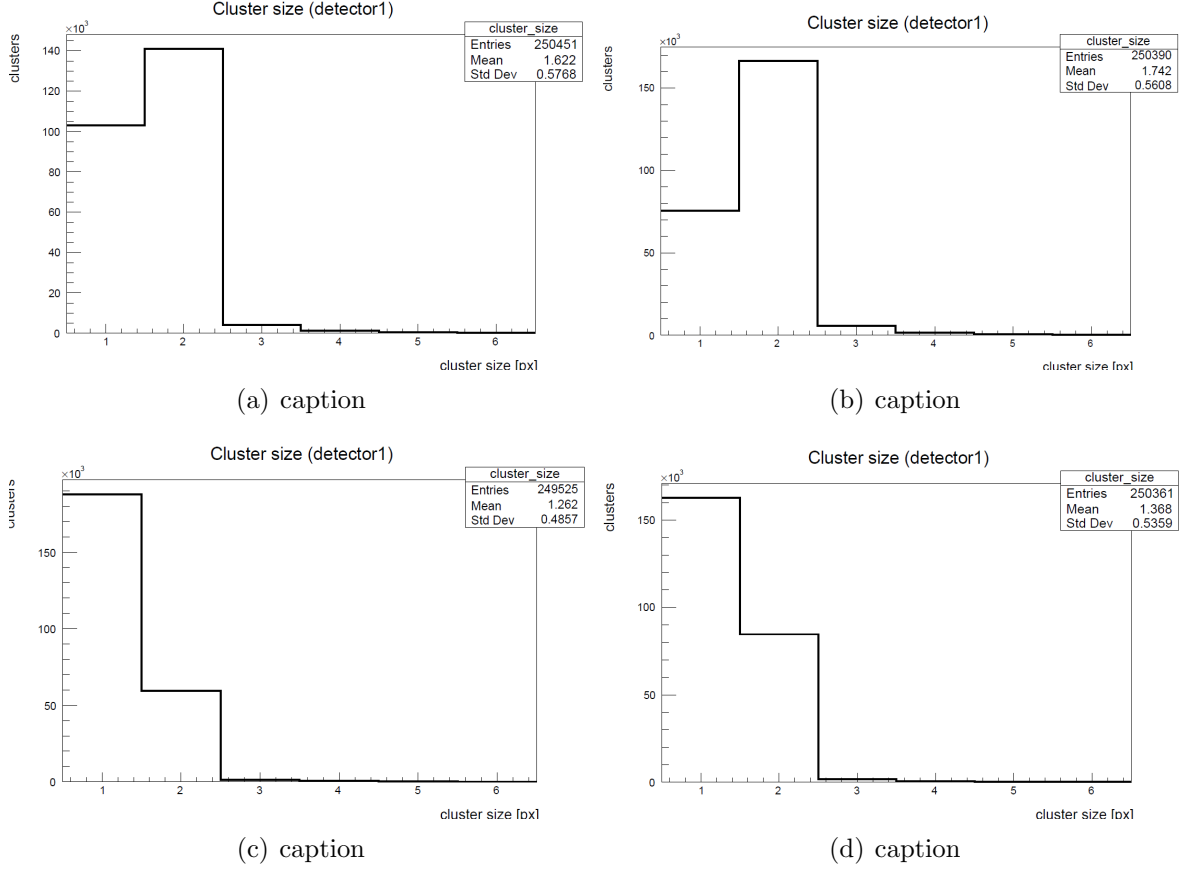


Figure 8: asf

Fig. 5.2 shows that for both simulated thresholds the mean cluster size increases from 1.622 to 1.742 for a $400\ \text{e}$ threshold and from 1.262 to 1.368 for a $1100\ \text{e}$ threshold when the resistivity is increased. This means that increasing the resistivity in general increases the mean cluster size as well. This makes sense as a higher resistivity means an overall lower doping concentration and therefore also a thicker depletion region at the same bias voltage. With a thicker depletion region more deposited charge carriers will experience drift towards the collection electrode due to the electric field in this region, thus increasing the collected charge and charge sharing.

Since the increased resistivity moves the mean cluster size towards the desired value of 2 — or 1.988 for the case of the test beam data —, the corresponding setups were

additionally rerun with adapted digitizer settings to see if the mean cluster can be improved even further. As it turns out the noise setting does not change the cluster size in any significant way, while increasing the gain shifts the cluster size even more towards the wanted value as Fig. 5.2 indicates. While the simulations in Fig. 5.2 were run with a gain of 1, the simulations in Fig. 5.2 were run with a gain of 1.3. This increases the mean cluster size from 1.742 to 1.859 for a 400 e threshold and from 1.368 to 1.437 for a 1100 e threshold.

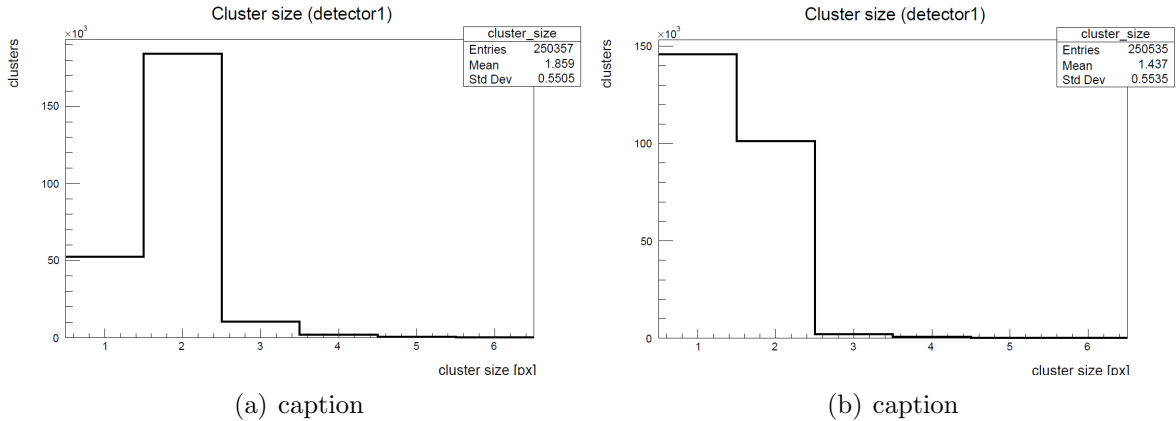


Figure 9: asf

6 Summary and Outlook

This study presents a simulation of the TelePix 180 nm HV-CMOS pixel sensor using a combination of three dimensional electrostatic field models simulated in TCAD and Monte Carlo simulation in Allpix². It describes the full simulation chain from geometry construction, particle energy deposition via Geant4, charge carrier propagation and signal digitization used in Allpix² as well as how to incorporate the TCAD models such that the simulation of charge carrier propagation is improved. The resulting simulations are compared to experimental data from test beam measurements at the DESY II test beam facility.

With the described simulation setup a rotational scan of the upper portion of the pixels is carried out. The results of the scan yielded simulations that make sense from a physics standpoint, but do not match the data received from the test beam measurements. Therefore an approach is presented to tune the simulations by comparing the mean cluster size of the simulation and the data, which yields a mean cluster size close to 2 at a beam incidence angle of 25° . It turns out that by increasing the resistivity in the simulated TCAD profiles and the gain amplification in the digitizer settings of the Allpix² configuration, the mean cluster size in the simulations can be increased towards the desired value of 2 in the data. While these results do not yet show a match to the

test beam data, they still suggest that further improvements can be made by increasing the resistivity of the TCAD profiles. This study therefore gives a basis for further investigations.

References

- [1] H. Augustin *et al.*, “Upgrading the beam telescopes at the desy ii test beam facility,” *Nuclear Instruments and Methods in Physics Research Section A: Accelerators, Spectrometers, Detectors and Associated Equipment*, vol. 1040, p. 167183, 2022.
- [2] R. Diener *et al.*, “The desy ii test beam facility,” *Nuclear Instruments and Methods in Physics Research Section A: Accelerators, Spectrometers, Detectors and Associated Equipment*, vol. 922, pp. 265–286, 2019.
- [3] J. Baudot *et al.*, “First test results of mimosa-26, a fast cmos sensor with integrated zero suppression and digitized output,” in *2009 IEEE Nuclear Science Symposium Conference Record (NSS/MIC)*, pp. 1169–1173, 2009.
- [4] C. Hu-Guo *et al.*, “First reticule size maps with digital output and integrated zero suppression for the eudet-jral beam telescope,” *Nuclear Instruments and Methods in Physics Research Section A: Accelerators, Spectrometers, Detectors and Associated Equipment*, vol. 623, no. 1, pp. 480–482, 2010. 1st International Conference on Technology and Instrumentation in Particle Physics.
- [5] S. Spannagel *et al.*, “Allpix2: A modular simulation framework for silicon detectors,” *Nuclear Instruments and Methods in Physics Research Section A: Accelerators, Spectrometers, Detectors and Associated Equipment*, vol. 901, pp. 164–172, 2018.
- [6] S. Agostinelli *et al.*, “Geant4—a simulation toolkit,” *Nuclear Instruments and Methods in Physics Research Section A: Accelerators, Spectrometers, Detectors and Associated Equipment*, vol. 506, no. 3, pp. 250–303, 2003.
- [7] J. Allison *et al.*, “Geant4 developments and applications,” *IEEE Transactions on Nuclear Science*, vol. 53, no. 1, pp. 270–278, 2006.
- [8] J. Allison *et al.*, “Recent developments in geant4,” *Nuclear Instruments and Methods in Physics Research Section A: Accelerators, Spectrometers, Detectors and Associated Equipment*, vol. 835, pp. 186–225, 2016.
- [9] D. Dannheim *et al.*, “Combining tcad and monte carlo methods to simulate cmos pixel sensors with a small collection electrode using the allpix2 framework,” *Nuclear Instruments and Methods in Physics Research Section A: Accelerators, Spectrometers, Detectors and Associated Equipment*, vol. 964, p. 163784, 2020.

- [10] P. Schütze *et al.*, “User Manual for the Allpix² Simulation Framework v2.3.1,” tech. rep., DESY, July 2022. <https://cern.ch/allpix-squared/usermanual/allpix-manual.pdf>.
- [11] R. Brun and F. Rademakers, “Root — an object oriented data analysis framework,” *Nuclear Instruments and Methods in Physics Research Section A: Accelerators, Spectrometers, Detectors and Associated Equipment*, vol. 389, no. 1, pp. 81–86, 1997. New Computing Techniques in Physics Research V.